Original Research Article

Pulmonary Circulation

Metabolic endophenotype associated with right ventricular glucose uptake in pulmonary hypertension

Samar Farha[1,2], Suzy Comhair[1], Yuan Hou[1], Margaret M. Park[1,3], Jacqueline Sharp[1,3], Laura Peterson[1], Belinda Willard[1], Renliang Zhang[1], Frank P. DiFilippo[4], Donald Neumann[4], W.H. Wilson Tang[1,3], Feixiong Cheng[1] and Serpil Erzurum[1,2]

[1]Lerner Research Institute, Cleveland Clinic, Cleveland, OH, USA; [2]Respiratory Institute, Cleveland Clinic, Cleveland, OH, USA; [3]Heart Vascular and Thoracic Institute, Cleveland Clinic, Cleveland, OH, USA; [4]Imaging Institute, Cleveland Clinic, Cleveland, OH, USA

Abstract

Alterations in metabolism and bioenergetics are hypothesized in the mechanisms leading to pulmonary vascular remodeling and heart failure in pulmonary hypertension (PH). To test this, we performed metabolomic analyses on 30 PH individuals and 12 controls. Furthermore, using 2-[18F]fluoro-2-deoxy-D-glucose positron emission tomography, we dichotomized PH patients into metabolic phenotypes of high and low right ventricle (RV) glucose uptake and followed them longitudinally. In support of metabolic alterations in PH and its progression, the high RV glucose group had higher RV systolic pressure ($p < 0.001$), worse RV function as measured by RV fractional area change and peak global longitudinal strain (both $p < 0.05$) and may be associated with poorer outcomes (33% death or transplantation in the high glucose RV uptake group compared to 7% in the low RV glucose uptake group at five years follow-up, log-ranked $p = 0.07$). Pathway enrichment analysis identified key metabolic pathways including fructose catabolism, arginine-nitric oxide metabolism, tricarboxylic acid cycle, and ketones metabolism. Integrative human protein-protein interactome network analysis of metabolomic and transcriptomic data identified key pathobiological pathways: arginine biosynthesis, tricarboxylic acid cycle, purine metabolism, hypoxia-inducible factor 1, and apelin signaling. These findings identify a PH metabolomic endophenotype, and for the first time link this to disease severity and outcomes.

Keywords

metabolomics, arginine, tricarboxylic acid cycle, FDG-PET scan, outcomes

Date received: 14 June 2021; accepted: 1 October 2021

Pulmonary Circulation 2021; 11(4) 1–12
DOI: 10.1177/20458940211054325

Pulmonary hypertension (PH) is a progressive and fatal disease characterized by abnormal remodeling of the pulmonary vasculature with excessive growth and dysfunction of pulmonary vascular endothelial and smooth muscle cells leading to increased pulmonary vascular resistance and right heart failure. PH patients have poor outcomes, with five-year survival around 60% despite advances in medical therapies.[1,2] Abnormalities in metabolism have been described in PH and speculated to contribute to development and/or progression of the disease.[3] A deep characterization using multi-omic studies is a strategy that has worked to identify biomarkers and novel therapies in other diseases, such as cancer treatment based on molecular profiling. This approach may similarly be revealing in PH given the known alterations in metabolic pathways and genetic profiles.[3–11] Changes in metabolism with decreased glycolytic oxidation and a shift to aerobic glycolysis as well as changes in fatty acid metabolism have been identified. These metabolic abnormalities are found in the lungs, heart, and skeletal muscles of patients as well as in cells derived from these organs.[3–10] Metabolomics signature of human pulmonary microvascular endothelial cells (hPMVEC) expressing two different mutations in bone

Corresponding author:
Samar Farha, Cleveland Clinic, 9500 Euclid Avenue, NB21, Cleveland, Ohio 44195, USA.
Email: farhas@ccf.org

morphogenic protein receptor (*BMPR*) 2 compared to cells without *BMPR2* mutations revealed aerobic glycolysis in *BMPR2* mutant hPMVEC, as well as abnormalities in the pentose phosphate pathway, increases in nucleotide salvage and polyamine biosynthesis pathways, decreases in carnitine and fatty acid oxidation pathways, and major alterations in the tricarboxylic acid (TCA) cycle.[4] In another study using metabolomics analysis, alterations in glycolysis and glucose metabolism, TCA pathway, and fatty acid metabolism were found in PH lung tissue.[7] Furthermore, the findings suggested that differences in metabolism in PH lungs were related to disease severity, i.e., increased glycolysis early in the disease and a switch to fatty acid metabolism later in advanced stages. However, whether PH outcomes are related to metabolomic signatures is unknown. In a previous report, we determined the metabolomic signatures at baseline in a group of PH patients and healthy controls prior to their participation in a double-blind, placebo-controlled trial using both non-targeted and confirmatory targeted analyses (Pulmonary Arterial Hypertension Treatment with Carvedilol for Heart failure, PAHTCH).[9,12,13] Using system biology analysis, we found differences in aspartate and asparagine metabolism, purine salvage, urea cycle, nicotinate metabolism, and sphingolipid metabolism as well as abnormalities in glutamate, isocitrate, cis-aconitate, glycine, arginine, citrulline, and purine metabolites.[9] In this study, outcomes of death or lung transplantation in the PH participants who were receiving standard of care were determined over five years follow-up. We found that metabolomic profiling and right ventricle (RV) glucose uptake measured by 2-[18F]fluoro-2-deoxy-D-glucose positron emission tomography (FDG-PET) scan were associated with outcomes in this cohort of PH patients. Integrative human interactome network analysis of plasma metabolomic data and existing transcriptome and proteome profiling data from PH patients identified unique metabolic, pathobiological pathways.

Methods

Study population

The study population was part of the PAHTCH, a randomized, placebo-controlled trial.[12] Only the baseline plasma samples from 30 PH individuals and 12 healthy age and sex-matched controls from the PAHTCH study were used to determine the metabolomic profiles. Participants were 18 to 65 years of age. We included patients with World Health Organization (WHO) groups 1, 3, and 4 and functional class I, II, or III. Diagnosis of pulmonary hypertension was confirmed by review of right heart catheterization showing a mean pulmonary arterial pressure of 25 mmHg or greater and pulmonary vascular resistance more than 3 Wood units.[12] All patients had wedge pressures less than 15 except for two patients: one patient with heritable PAH had a wedge pressure of 16 on initial right heart catheterization and one patient with mixed PH diagnosed as idiopathic PAH as the precapillary component was deemed out of proportion and had a wedge pressure of 21. A full set of inclusion and exclusion criteria are provided in NCT01586156. The study was approved by the Institutional Review Board, and written informed consent was obtained from all participants. Blood samples were obtained from all participants after an overnight fast. Plasma was separated and stored at –80°C for analyses. The study intervention lasted for six months, and then participants continued on their standard of care. For the purpose of this study, we used baseline visit samples and data as well as echocardiograms done at the six months visit. In addition, we collected echocardiogram measurements of RV systolic pressure (RVSP) and RA pressure (RAP) from the medical records at five years from the subject enrollment date ($n = 16$) to assess disease progression. We evaluated outcomes of death or lung transplantation in this cohort after five years of follow-up from date of enrollment by reviewing the electronic medical records. Only one patient was lost for follow-up. All other subjects had a known status at five years from enrollment in the parent study.

Non-targeted metabolomic analysis

Non-targeted metabolomics and lipidomics analysis were performed at Metabolon, Inc (Durham, NC). The details of analytical platform and data curation have been described in detail previously.[14] The global, unbiased platform was based on a combination of three separate platforms: ultrahigh performance liquid chromatography/tandem mass spectrometry (UHPLC/MS/MS) optimized for basic species, UHPLC/MS/MS optimized for acidic species, and gas chromatography/mass spectrometry (GC/MS). The major components of the analytic process and the analytic platform have been described in detail in previous publications.[14–16] UHPLC/MS/MS analysis utilized a Waters Acquity UHPLC (Waters Corporation, Milford, MA) coupled to an LTQ mass spectrometer (Thermo Fisher Scientific, Inc., Waltham, MA) equipped with an electrospray ionization source. Two separate injections were performed on each sample: one optimized for positive ions and one for negative ions. Derivatized samples for GC/MS were analyzed on a Thermo-Finnigan Trace DSQ fast-scanning single-quadrupole MS operated at unit mass resolving power. Chromatographic separation followed by full scan mass spectra was carried to record retention time, mass to charge (m/z) ratio, and MS/MS of all detectable ions present in the samples. Compounds were identified by automated comparison to Metabolon's reference library entries. Identification of known chemical entities was based on comparison with Metabolon's library entries of purified standards.

Confirmatory targeted metabolomic analysis

Plasma amino acid concentrations were measured following ortho-phthalaldehyde derivatization using a fluorescent detector and HPLC (Agilent 1100 series, Agilent technologies, Wilmington, DE) as described previously.[17] Plasma total homocysteine, cysteine, and glutathione concentrations were measured using a thiol-SBD derivative on an HPLC as described.[18] Arginine metabolomic profiles were measured as previously described.[19] In brief, each sample solution was injected onto a HPLC column and ADMA, L-arginine, L-ornithine, and L-citrulline levels were quantified by LC/ESI/MS/MS analysis using an ABI 365 triple quadrupole mass spectrometer (Applied Biosystems Inc., Foster City, CA, USA) with Ionics EP 10+ redesigned source (Concord, Ontario, Canada) and electrospray ionization (ESI) needle connected to an Aria LX4 series multiplexed HPLC system with Flux pumps (Cohesive Technologies, Franklin, MA).

Echocardiogram

Doppler echocardiography was performed as previously described in this cohort.[12] Right ventricular function was assessed via measurement of RV fractional area change (RVFAC), myocardial performance index of the RV, tricuspid annular plane systolic excursion (TAPSE), tissue Doppler-derived systolic velocity of the lateral tricuspid annulus, and longitudinal strain by two-dimensional speckle tracking technique. The calculation of RVFAC was based on the following formula: RVFAC (%) = (RV end-diastolic area – RV end-systolic area)/RV end-diastolic area × 100.

Two Dimensional (2D) Speckle –Tracking Echocardiography (STE) was used for the evaluation of myocardial function.[20–24] Strain values were determined for each segment (segmental strain) globally and regionally. Average RV peak global longitudinal strain or global strain, which refers to the average longitudinal strain value of all six segments of the myocardium, was assessed as a measure of right ventricular function over time of the study.

FDG-PET to determine cardiac glucose metabolism

Cardiac FDG-PET scans were conducted on fasting individuals with PH at baseline. All individuals fasted 8 h prior to and during the study; they were then injected with 370 MBq (10 mCi) FDG, and the scan was performed 1.5 h post-injection. Finger stick blood sugar was measured to assure fasting state (blood sugar <120 mg/dl). Data were acquired and analyzed as described in the previous report of this population.[12,13]

Analysis

Quantitative characteristics of the study population have been previously reported using mean and standard deviation, while categorical characteristics described using number and percent.[25] Standard statistical analyses were performed in ArrayStudio on log transformed data. For those analyses not standard in ArrayStudio, the programs R (http://cran.r-project.org/) or JMP (JMP Pro, version 15.2, SAS Institute) were used. Log-ranked analysis was performed for transplant-free survival analysis between the 2 FDG RV/LV uptake (high and low) groups over the five years follow-up with BH correction.[26] The survival analysis was performed using the Survival and Survminer packages in R v4.1.0 (https://www.r-project.org).

The observed relative concentration of each biochemical was log transformed and imputed with minimum observed values for that compound.[14] A Welch two-sample t-test was used to identify biochemicals that differed significantly between PH subjects and healthy controls. A probability of 0.05 was used as evidence of statistically significant difference in the population means. An estimate of the false discovery rate (q value) was calculated to take into account the multiple comparisons. Principal components analysis was used for the unsupervised analyses of metabolites to determine "separation" of PH and healthy controls. Pathway enrichment was performed to identify pathways that are significantly different between PH and controls (Metabolon Inc®. proprietary software, Metabolync®). A pathway enrichment value greater than one indicates that the pathway contains more compounds relative to the study overall, suggesting that the pathway may be a target of interest for pathobiology of PH (Enrichment: [no. of significant metabolites in pathway (k)/total no. of detected metabolites in pathway (m)]/(total no. of significant metabolites (n)/total no. of detected metabolites (N)) (k/m)/(n/N). T-distributed stochastic neighbor embedding (tSNE) analysis was performed by tsne v0.1-3 package in R 4.0.3 platform.

To build a comprehensive human protein–protein interactome (PPI), we assembled data from 18 common databases with five types of experimental evidences: (1) binary PPIs tested by high-throughput yeast-two-hybrid (Y2H) systems[27–29]; (2) kinase-substrate interactions by literature-derived low-throughput and high-throughput experiments from PhosphoNetworks,[30] KinomeNetworkX,[31] Human Protein Resource Database (HPRD),[32] PhosphositePlus,[33] DbPTM 3.0,[34] and Phospho ELM[35]; (3) carefully literature-curated PPIs identified by affinity purification followed by mass spectrometry (AP-MS), Y2H and by literature-derived low-throughput experiments, and protein three-dimensional structures from BioGRID,[36] PINA,[37] Instruc,[38] MINT,[39] IntAct,[40] and InnateDB;[41] (4) signaling network by literature-derived low-throughput experiments as annotated in SignaLink2.0;[42] and (5) protein complexes data (56,000 candidate interactions) identified by a robust affinity purification-mass spectrometry methodology were collected from BioPlex V2.[43] The genes were mapped to their Entrez ID based on the NCBI database as well as their official gene symbols based on GeneCards (http://www.genecards.org/).

Duplicated pairs were removed. Hence, inferred data, such as evolutionary analysis, gene expression data, and metabolic associations, were excluded. The resulting updated human interactome used in this study includes 351,444 PPIs connecting 17,706 unique proteins. The details are provided in our recent studies.[29,44]

To build a comprehensive metabolite-enzyme network, we assembled data from three commonly used metabolism databases: Kyoto Encyclopedia of Genes and Genomes (KEGG),[45] Recon3D,[46] and human metabolic atlas.[47] We then mapped the differentially expressed proteins (enzymes) and significant metabolites into the metabolite-enzyme network to identify the dysregulated metabolism pathways in PAH.

To perform integrative network analyses, we used a PH dataset from GEO database (GSE113439).[48] In the original study, 26 explanted lungs collected from 15 PH patients and 11 healthy controls underwent microarray analysis (Affymetrix).[48] The microarray expression profiles from these samples were characterized, and the fold change (FC) and adjusted p-value (FDR) were calculated by limma and GEO2R package. We used the transcriptome data with metabolome for integrative analyses of PH pathways.

Results

Participants

Thirty subjects with PH and 12 healthy controls were enrolled in this study. The study population was described in a prior report.[12] Historical hemodynamics showed mean pulmonary arterial pressure (mPAP) of 49 ± 14, pulmonary vascular resistance (PVR) of 8.2 ± 4.7, wedge pressure of 10.2 ± 3.5, and thermodilution CO of 5.6 ± 1.6. We have previously shown that right ventricular (RV) glucose uptake is higher in PH compared to controls and correlates with echocardiographic measures of RV function and NT-pro BNP[12,13] but not with six-minute walk distance. These associations persisted at the six-month follow-up visit with RV glucose uptake correlating with RV function and NT-pro BNP (RVSP (mmHg): $R = 0.5$, $p = 0.002$; RV strain (%): $R = 0.7$, $p < 0.0001$; RV FAC (%): $R = -0.4$, $p = 0.03$; NT-pro BNP (pg/ml): $R = 0.6$, $p = 0.0003$). However, a significant heterogeneity of RV glucose uptake among PH participants was noticed. Hence, PH patients were dichotomized to a high or low RV glucose uptake phenotype based on the median RV/LV FDG uptake of 0.8 (Fig. 1). The high RV glucose uptake group had a more severe disease phenotype, with higher RVSP, right atrial (RA) pressure, endothelin-1 levels, and worse RV function as measured by RV strain and RV fraction area contraction (FAC) (Table 1) (Fig. 1). At the six-month follow-up visit, the high RV glucose uptake group had higher RVSP compared to the low RV glucose uptake group: (RVSP (mmHg): low RV glucose uptake PH group 47 ± 18, high RV glucose uptake PH group 72 ± 27, $p = 0.01$). Sixteen patients had echocardiograms at five years follow-up and there was no significant difference in RVSP between the two groups (RVSP (mmHg): low RV glucose uptake PH group 63 ± 18, high RV glucose uptake PH group 78 ± 33, $p = 0.3$). Although there were no significant changes in RVSP in either group from baseline to five-year follow-up, the high RV glucose uptake phenotype tended to associate with worse clinical outcome as measured by death or transplant on follow-up over five years with five patients (33% of patients) getting transplanted or dying in the high RV glucose uptake group compared to one patient (7%) in the low RV glucose uptake group (log-ranked $p = 0.07$) (Figs. 2 and 3).

Metabolic profiling of the high and low RV glucose uptake PH subgroups

To identify the metabolomic endophenotype of the high RV glucose uptake PH group to help detect novel biomarkers and enhance our understanding of disease pathophysiology, we compared targeted and non-targeted metabolomics among the high and low RV glucose uptake PH groups and healthy controls. A total of 1,957 biochemicals, 1,583 compounds of known identity (named biochemicals) and 374 compounds of unknown structural identity (unnamed biochemicals) were measured. As previously reported by our group, there were significant differences between PH and controls.[9] When comparing high and low RV glucose uptake PH groups to healthy controls, 119 metabolites were significantly different in the high RV glucose uptake PH group compared to healthy controls (Fig. 3). Most biochemicals were involved in the TCA cycle and amino acid metabolism, mainly glutamate, aspartate, tryptophan, and tyrosine and arginine/urea cycle as well as nucleotide metabolism (Supplementary Table 1). We used t-distributed stochastic neighbor embedding (t-SNE) to visualize the individual participants from the different subgroups based on the 119 differential metabolites found in the high RV glucose uptake PH group. Participants were separated into 3 subgroups based on the 119 specific metabolites (Fig. 4). Pathway enrichment analysis revealed significant differences in the high RV glucose uptake group compared to healthy controls not seen in the low RV glucose uptake group (Fig. 4). The differentially expressed metabolites in the high RV glucose uptake group were significantly enriched in four main metabolic pathways ($FDR < 0.05$): fructose catabolism (adenosine 5-diphosphate (ADP), fructose, glycerate), ketone bodies synthesis and metabolism (adenosine 5′-monophosphate (AMP), 3-hydroxybutyrate (BHBA)), TCA cycle (ADP, malate, citrate, isocitrate), and eNOS activation (ADP, arginine, heme) (Fig. 4).

Targeted metabolomics confirmed the findings from non-targeted analysis and revealed significant differences in the urea cycle/arginine-nitric oxide pathway. The high

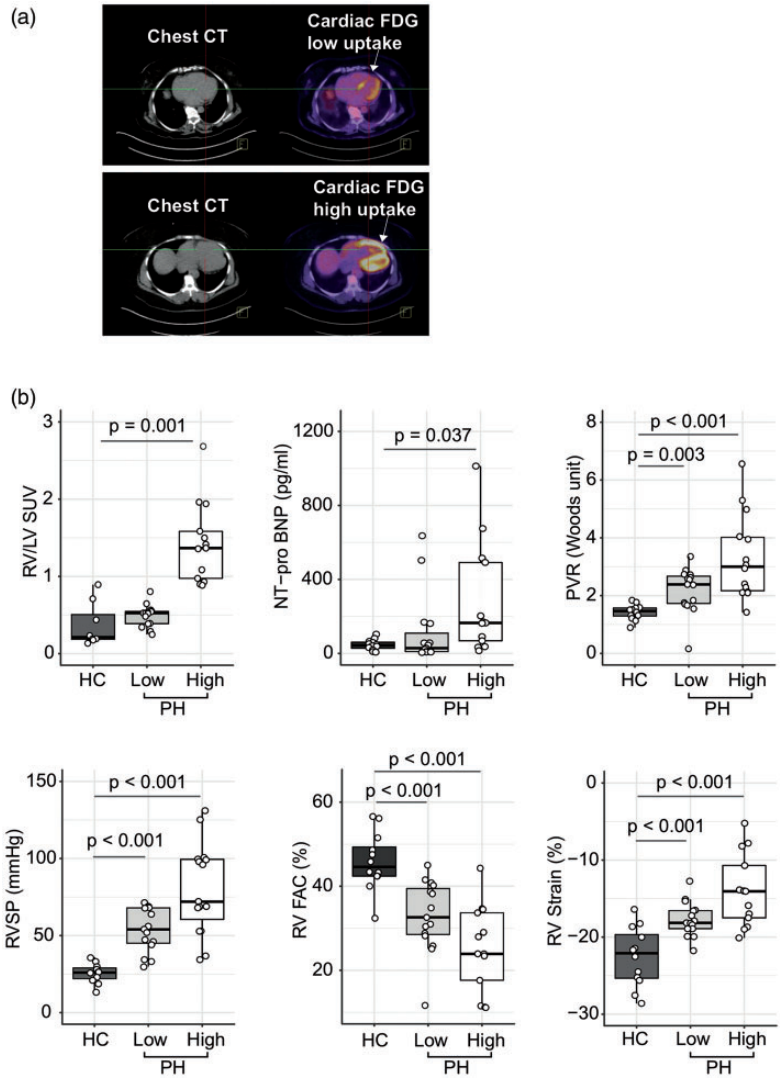

Fig. 1. Right ventricle (RV) 2-[18F]fluoro-2-deoxy-D-glucose (FDG) positron emission tomography (PET) uptake identifies a PH phenotype with worse RV function. RV FDG uptake on PET imaging is heterogeneous among PH patients with higher RV FDG uptake associated with a clinical PH phenotype of worse RV function and more severe disease. (a) Cardiac FDG PET scan contrasting RV glucose uptake in two PH subjects (high and low RV glucose uptake). Each panel depicts the CT scan image with its corresponding PET scan image. Lower panel shows increased RV glucose uptake in PH compared to normal RV glucose uptake levels in upper panel. White arrow pointing at RV. (b) There are significant differences in clinical parameters of disease severity and RV function among healthy controls and PH patients with low and high RV glucose uptake. The data are represented as a boxplot where the middle line is the median, the lower and upper edges of the box are the first and third quartiles, the whiskers represent the interquartile range (IQR) $\times 1.5$. Each dot denotes individual observations. Two-tailed t-test was used to evaluate significant difference at $p < 0.05$. HC: healthy controls; High: high RV glucose uptake PH group; Low: low RV glucose uptake PH group.

RV glucose uptake group had significantly lower arginine and citrulline levels compared to the healthy controls (arginine (μM): controls 91 ± 35, high RV glucose uptake PH group 58 ± 17, t-test, $p = 0.004$ and citrulline (μM): controls 41 ± 9, high RV glucose uptake PH group 34 ± 6, t-test, $p = 0.018$) (Fig. 4). Arginine methylation products have different functions, one of which is inhibition of nitic oxide synthetase. There are different methylation products: mono-methylated (MMA), symmetric demethylated (SDMA), and asymmetric demethylated (ADMA). ADMA was increased in both PH groups compared to controls (ADMA (μM): controls 0.41 ± 0.04, low RV glucose PH uptake group 0.49 ± 0.09, high RV glucose uptake PH group 0.51 ± 0.08, ANOVA $p = 0.005$) (Fig. 4). Global arginine bioavailability ratio (GABR, defined as arginine/[ornithine + citrulline]) was lowest in the high glucose uptake group (GABR: controls 1.0 ± 0.3, low RV glucose uptake PH group 0.9 ± 0.4, high RV glucose uptake PH group 0.7 ± 0.3, $p = 0.05$). As shown previously, arginine and GABR correlated with RV glycolysis (Arginine: $R = -0.4$, $p = 0.01$ and GABR: $R = -0.4$, $p = 0.02$).

In addition, non-targeted metabolomics showed significant changes in amino acids between the high and low glucose uptake PH groups. There were significant changes in

Table 1. Clinical phenotype of high and low RV glucose uptake PH groups.

	Low RV glucose uptake group	High RV glucose uptake group	p-value
	N = 15	N = 15	
Age (years)	46 ± 11	43 ± 13	0.5
Race			0.4
Caucasian, n (%)	12 (80%)	11 (73.33%)	
African American, n (%)	2 (13.33%)	2 (26.67%)	
Asian, n (%)	1 (6.67%)	0	
Gender			0.2
Female, n (%)	12 (80%)	9 (60%)	
Male, n (%)	3 (20%)	6 (40%)	
Height (cm)	166 ± 11	168 ± 8	0.6
Weight (kg)	79 ± 18	86 ± 21	0.3
Temperature (F)	97.1 ± 0.7	97.5 ± 0.7	0.1
Classification of pulmonary hypertension			0.4
Pulmonary arterial hypertension, n (%)			
Idiopathic	4 (26.67%)	5 (33.33%)	
Heritable	4 (26.67%)	8 (53.33%)	
Associated	4 (26.67%)	1 (6.67%)	
Pulmonary hypertension due to lung diseases and/or hypoxia, n (%)	2 (13.33%)	0	
Chronic thromboembolic pulmonary hypertension, n (%)	1 (6.67%)	1 (6.67%)	
Pulse (beats/min)	79 ± 7	80 ± 8	0.8
O_2 Saturation (% of Hgb)	96 ± 3	96 ± 3	0.9
Echocardiogram			
LA area (cm^2)	17 ± 3	18 ± 4	0.9
LV end diastolic diameter (cm)	4.8 ± 0.5	4.1 ± 0.7	0.007
LV end systolic diameter (cm)	3.0 ± 0.7	2.3 ± 0.5	0.007
LVEF (%)	56 ± 8	62 ± 7	0.05
RA area (cm^2)	17 ± 4	24 ± 7	0.006
RA pressure (mmHg)	5.7 ± 1.8	8.0 ± 4.9	0.1
RV end diastolic area (cm^2)	25 ± 6	34 ± 9	0.005
RV end systolic area (cm^2)	17 ± 5	26 ± 8	0.004
RVSP (mmHg)	54 ± 14	80 ± 30	0.005
RV fractional area change (%)	33 ± 9	25 ± 10	0.04
LV stroke volume (ml)	67 ± 16	58 ± 18	0.2
LV cardiac output (l/min)	5.2 ± 1.7	4.4 ± 1.4	0.2
RV peak global longitudinal strain (%)	−18 ± 2	−14 ± 5	0.02
LV peak global longitudinal strain (%)	−18 ± 3	−18 ± 3	0.8
6 minute-walk distance (m)	471 ± 134	451 ± 100	0.7
NT-proBNP (pg/ml)	123 ± 53	857 ± 1703	0.1
WHO functional class (I/II/III)	3/8/4	0/13/2	0.1

RV: right ventricle; LV: left ventricle; LA: left atrium; LVEF: left ventricle ejection fraction; RA: right atrium; RVSP: right ventricle systolic pressure; WHO: World Health Organization; NT-proBNP: N-terminal pro–B-type natriuretic peptide; O_2: oxygen, Hgb: hemoglobin.

glutamate metabolism, with increased levels of glutamate, N-acetylglutamate, 4-hydroxyglutamate, and beta-citrylglutamate in the high RV glucose uptake group compared to controls (FDR $p < 0.05$) and a reduction in glutamine and S-1-pyrroline-5-carboxylate (FDR $p < 0.05$). Glutamate and beta-citrylglutamate were increased in the low RV glucose uptake PH group compared to controls (FDR $p < 0.05$). Targeted metabolomics analysis confirmed the increase in glutamate in PH (Glutamate (μM): controls 39 ± 13, low RV glucose uptake PH group 63 ± 28, high RV glucose uptake PH group 68 ± 35, $p = 0.03$) (Fig. 4).

An integrative network analysis reveals existing and novel metabolic pathways in PH

To investigate the molecular mechanism of metabolic phenotypes of PH, we performed an integrative network analysis for metabolomics and previously published transcriptomic[48] and proteomic datasets[9] in PH patients compared to healthy controls. We found that 26 specific metabolites in the high RV glucose uptake group were regulated by 162 enzymes in metabolite-enzyme networks, and 86 enzyme-coding genes were differentially expressed in the lungs of PH patients compared to healthy controls

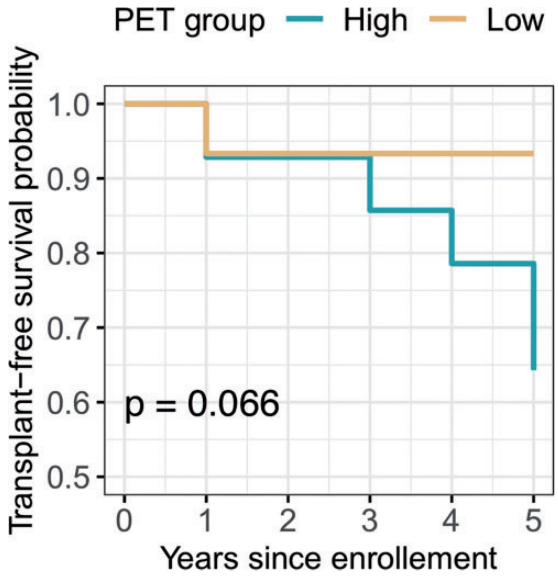

Fig. 2. Kaplan-Meier transplant-free survival curve of PH patients with high and low RV FDG PET uptake. Log-ranked analysis was performed to assess transplant-free survival between the two FDG RV/LV uptake (high and low) groups over five-year follow-up. Patients were followed over five years from date of enrollment in the parent study with only one patient lost for follow-up. All other subjects had a known status at follow-up. Events were defined as death or transplantation.

(GSE113439).[48] Using gene pathway enrichment analysis, we found that 86 differentially expressed enzyme-coding genes were significantly enriched in the TCA cycle as well as the arginine and proline pathways, mechanistically supporting the metabolic phenotype (Supplementary Fig. 2). Furthermore, 321 neighbors of the 86 differentially expressed enzyme-coding genes in the human interactome were enriched in the arginine biosynthesis pathway, the TCA cycle, HIF-1, and apelin signaling pathways. The network of the 26 metabolites specific to the high glucose uptake phenotype with their enzymes and their neighborhood are shown in Fig. 5. We found that arginine was highly connected to nitric oxide synthetase 3 (NOS3) and AKT1 which are significantly lower at RNA and protein levels in PH.[48] Low glutamine level and high glutaminase (GLS) are found in PH and may be associated with accumulation of glutamate in the mitochondria, which would feed the TCA cycle (Fig. 6).

Discussion

This study identifies a unique metabolic signature that is associated with more severe disease and worse clinical outcomes in a subgroup of PH patients. The median RV/LV cut-off of 0.8 separated the PH patients into high and low RV glucose uptake and tended to associate with poorer outcomes (33% death or transplantation in the high glucose RV uptake group compared to 7% in the low RV glucose uptake group at five years follow-up, log-ranked $p = 0.07$).

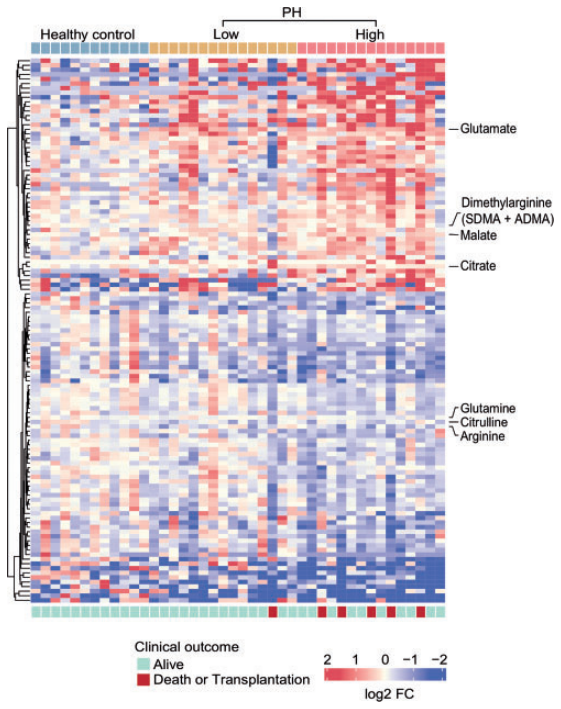

Fig. 3. Heatmap illustrating the metabolic landscape in PH based on RV glucose uptake. In total, 119 differential metabolites that are significantly different in high RV glucose uptake PH group compared to healthy control group are displayed in the heatmap. The rows on top of heatmap show the individual subjects grouped by disease phenotypes, including health controls, low *versus* high RV glucose uptake PH group. There were no differences in age and gender distribution among the three groups. Clinical outcome (bottom row) defined as death or transplantation at 5 years follow up is shown outlining worse outcome in the high RV glucose uptake PH group. The gradient color bar from blue to red shows the log2 fold change (FC) of the differential metabolites in healthy control compared to low or high RV glucose PH patients (blue for lower levels and red for higher levels of the different metabolites compared to levels in healthy controls). Highlighted on the side of the heatmap are specific metabolites of the urea cycle arginine-nitric oxide pathway and the amino acids glutamine and glutamate that were confirmed by targeted measurements as shown in Fig. 4. HC: healthy controls; High: high RV glucose uptake PH group; Low: low RV glucose uptake PH group.

This metabolic signature is characterized by high RV glucose uptake by FDG-PET imaging and alterations in circulating metabolites particularly in fructose catabolism, ketone bodies synthesis and metabolism, TCA cycle, and eNOS activation. While previous studies have shown significant metabolic alterations in PH, our findings highlight the metabolomic heterogeneity among PH patients and identify a signature that may be associated with worse outcome.

In response to the increased pulmonary pressure, the RV remodels with changes in structure and shape as well as undergoes cellular changes with cardiomyocyte hypertrophy and reactivation of a fetal program of gene expression. This is similar to what is described in the left ventricle (LV) in left heart failure. While initially it is compensatory, over time remodeling becomes maladaptive and contributes to the

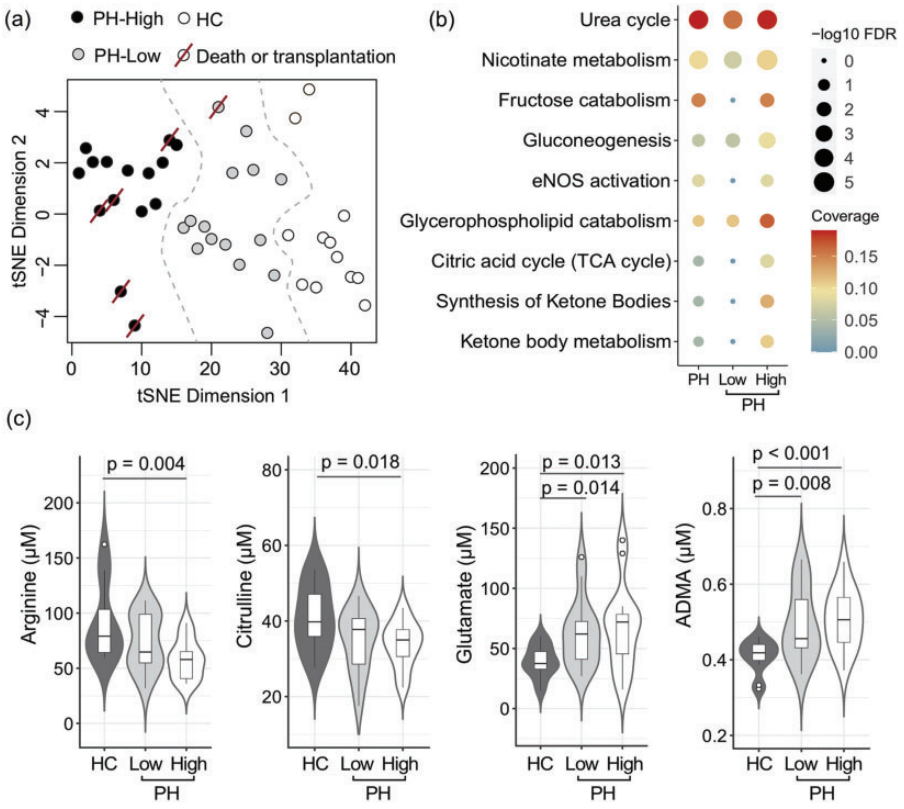

Fig. 4. Metabolic signature of PH endophenotype associated with worse clinical outcome. (a) A tSNE plot shows patient stratification of high RV glucose uptake PH and low RV glucose PH subjects and healthy controls, using 119 differential metabolites identified in Fig. 3. Worse outcomes noted in the high RV glucose uptake group. (b) Metabolic pathway enrichment analysis for the differential metabolites in the PH group including all 30 PH subjects and in low and high RV glucose groups compared to healthy controls. The high RV glucose uptake phenotype has a specific metabolic signature with significant differences in the TCA cycle and nitric oxide pathway as well as fructose catabolism and ketones metabolism. FDR: false discovery rate (adjusted p-values) during metabolic pathway enrichment analysis. Coverage denote the proportion of overlap between the identified differential metabolites and the known metabolites in a specific metabolic pathway. (c) Targeted measurements validate findings from non-targeted analysis with significant changes in arginine, citrulline, glutamate and ADMA levels in the high RV uptake PH group compared to healthy controls. Two-tailed t-test was used to evaluate significant difference at $p < 0.05$. The data are represented as a boxplot with a underlaid violin plot where the middle line is the median, the lower and upper edges of the box are the first and third quartiles, the whiskers represent the interquartile range (IQR) $\times 1.5$. HC: healthy controls; High: high RV glucose uptake PH group; Low: low RV glucose uptake PH group.

energy deficit of the failing heart. In both LV and RV failure, mitochondrial and metabolic abnormalities have been described with a metabolic switch from fatty acid oxidation to glycolytic carbohydrate metabolism.[49] With the switch to aerobic glycolysis, fewer ATP molecules/glucose molecule are produced but more ATP per mole of oxygen compared to fatty acid metabolism. This leads to a metabolic vicious circle that exacerbate cardiac dysfunction, failure, and death. To offset the increased glycolysis, glucose uptake is accelerated and can be assessed by PET. Cardiac PET scans are mainly used in left-sided disease to assess myocardial perfusion and viability. In one study looking at PET scans in heart failure with low ejection fraction, RV glucose uptake was found to correlate with RV pressure overload and to have significant prognostic value.[50] In PAH, RV glucose uptake has been shown to correlate with RV function and pressure overload.[13,51–53] Here we show a cutoff of RV/LV FDG PET that may be associated with worse clinical outcomes with increased transplant and death in the PH group with higher RV glucose uptake. When looking at noninvasive clinical markers of disease severity in our cohort, there were no differences in NT-pro BNP, six-minute walk distance, or WHO functional class between the high and low RV glucose uptake groups, suggesting that RV glucose uptake is an important predictor of outcome in PH, especially in patients on pulmonary vasodilator therapy. This is a small cohort of patients, and larger studies are needed to confirm the association between RV FDG PET uptake and patients' outcomes.

The metabolic endophenotype associated with the elevated RV glucose uptake showed dysregulation of the arginine-nitric oxide pathway. We and others have shown abnormalities in mitochondrial arginine metabolism in PH with decreased NO production, inactivation of eNOS, decreased arginine availability, and increased arginase 2 activity.[3] Here, we show a difference in arginine metabolism

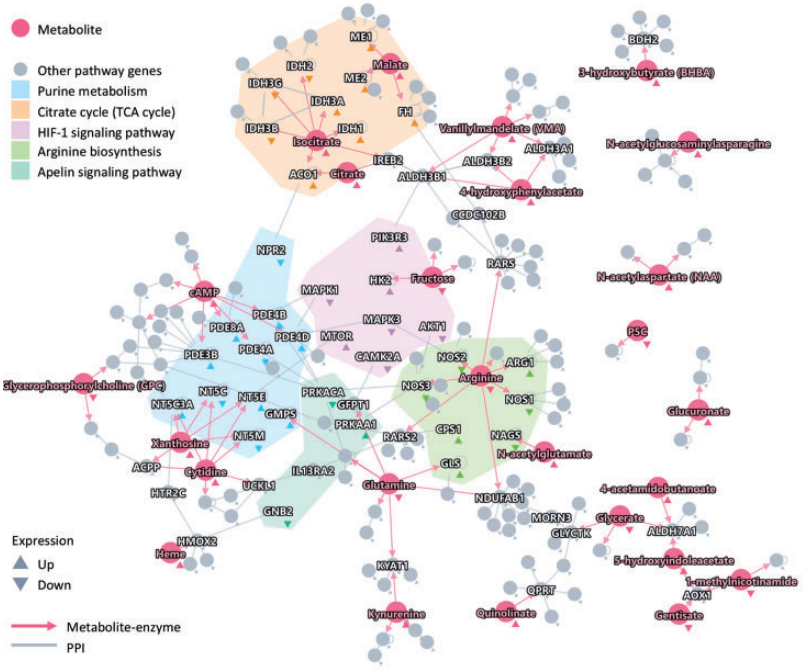

Fig. 5. An integrative human protein-protein interactome network analysis of metabolomics and proteomics profiling data revealing novel metabolic endophenotypes in PH patients. A protein-protein-metabolite network highlighting existing and novel metabolic pathways for high RV glucose PH. In total, 26 differential metabolites with well-known metabolic enzymes for high RV glucose PH patients were shown. The colored shadow shows the significant metabolic pathways (Supplementary Fig. 2B) enriched by differentially expressed enzyme-coding genes using microarray analysis (Affymetrix) of explanted lungs collected from 15 PH patients and 11 healthy controls (GEO ID: GSE13439, see Methods)[48] and their neighbors in the human protein-protein interactome network. The red directed edges denote the physical metabolite-enzyme interactions. Gray edges denote physical protein-protein interactions (PPIs). Up and Down show up-regulation and down-regulation during differential expression analysis.

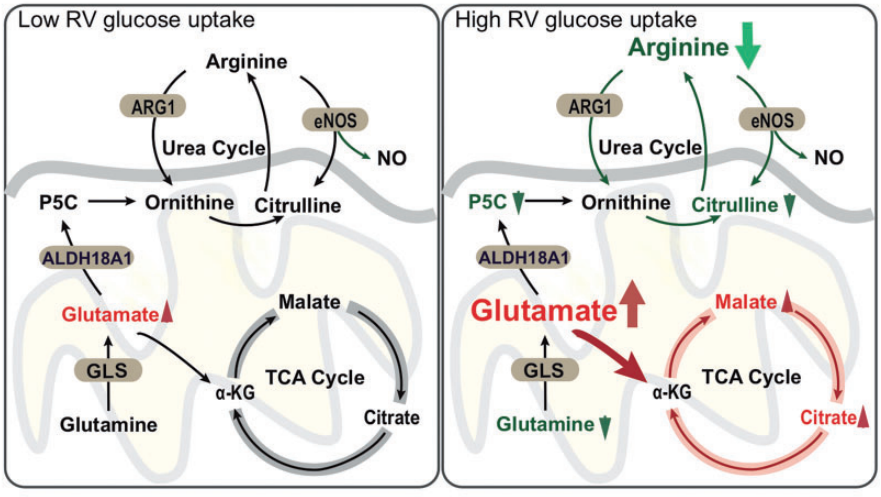

Fig. 6. Elevated RV glucose uptake identifies a PH endophenotype with unique alterations in cellular metabolism. Integrative network analysis incorporates non-targeted metabolomics and known physical metabolite-enzyme network data (using databases: Kyoto Encyclopedia of Genes and Genomes (KEGG), Recon3D, and Human Metabolic Reaction 2 (HMR2), see Methods). Glutamate and arginine play a key role in high RV glucose uptake PH phenotype. TCA is important for energy and is also an important source of substrates to synthesize amino acids, proteins, and DNA. It is closely related to the urea cycle and glutamine metabolism. Conversion of glutamine to glutamate is a source of amino acid substrate to enter TCA in proliferative/glycolytic cells. Ornithine produced by ARG2 is another key pathway to provide a steady source of glutamate to enter TCA *via* α-ketoglutarate (αKG). These changes in metabolism with decreased arginine bioavailability reflect the bioenergetic and biosynthetic demands of highly proliferative cell growth. Targeting these metabolic pathways offer appealing therapeutic options in PH that need to be further evaluated. Red denotes elevated metabolites, green decreased metabolites with $p < 0.05$. Shaded ellipses mark enzymes in the pathway. GLS: glutaminase; eNOS: endothelial nitric oxide synthetase; ARG2: arginase 2. ALDH18A1.

between two PH phenotypes highlighting disease heterogeneity with a more profound dysregulation in the high RV glucose uptake phenotype. In fact, lower arginine bioavailablility and decreased citrulline and nitric oxide production identify a metabolic PH phenotype associated with increased RV glycolysis, worse RV function, and poor outcome. These changes are associated with increased glutamate. Put together, the alterations in arginine metabolism in the high RV glucose uptake group contribute to increased pulmonary vasoconstriction through decreased NO and provide substrates for the TCA cycle to fuel the hyperproliferative pulmonary endothelial cells. It is unclear whether the differences in metabolism among the two PH phenotypes reflect different stages in disease progression or differences in metabolic pathobiological pathways. In addition, our findings share similarities to what has been described in left heart failure literature where studies showed a diverse array of metabolic alterations.[54] Cheng et al. identified a metabolite panel in left heart failure that has a diagnostic value similar to B-type natriuretic peptide and a prognostic value better than traditional biomarkers.[55] Whether the identified metabolic signature is specific to PH or reflect progressive heart failure, left or right sided will need to be further elucidated. Nonetheless, findings support that PH is a heterogeneous disease and emphasize the need for better biomarkers to improve diagnosis and enhance prognostication, and a multi-omics approach to direct PH therapy.

We further performed an integrative human protein–protein interactome network analysis of metabolomics, transcriptomics, and proteomics data to investigate underlying metabolic pathobiological pathways in PH associated with high RV glycolysis. We identified metabolic enzyme-encoding genes related to a high RV glycolysis phenotype that were highly enriched in the arginine biosynthesis pathway, TCA cycle, and HIF-1α and apelin signaling pathways. Transcriptomics showing decreased NOS3 and AKT1 and increased GLS support proteomics and metabolomics findings in PH of nitric oxide and arginine pathways downregulation and altered glutamate metabolism. Apelin signaling has been shown to be altered in PH with lower plasma levels and decreased expression in the PH lungs. Apelin signaling modulates vascular tone causing vasodilation through eNOS activation and NO signaling and increases cardiac contractility. In addition, apelin signaling is regulated by hypoxia. Here, we found both HIF-1α and apelin pathways significantly enriched in the high RV glucose uptake PH group[56–59] with increased hexokinase II and AKT1.

Circulating metabolites reflect the metabolic changes in the pulmonary vasculature (PV) and RV in PH as previously shown.[5–7,9,60] The roles of these metabolites as potential biomarkers of RV-PV dysfunction and to guide therapy need further appraisal. This study has limitations. The analysis was done post hoc after discovering the two PH metabolic phenotypes based on RV FDG PET uptake and the sample size is relatively small (N = 30). This could explain the lack of statistical significance in transplant-free survival between the two groups. Similarly, some alterations in metabolites may have not been detected because of the small sample size. In addition, potential literature bias of the human interactome and database-curated metabolite-enzyme association network may influence our network-based findings. Further validation of significant metabolites using large-scale independent PH cohorts is warranted as well as functional confirmation of network-predicted metabolites and enzymes in several identified key metabolic pathways using human cells or animal models. Although data from this small cohort cannot differentiate whether this metabolic PH phenotype represent patients at a more advanced stage in their disease or inherent metabolic heterogeneity among PH patients, the findings point to a unique metabolic PH phenotype and support the concept that metabolic therapeutic approaches should be studied in PH.

Author contributions

Conceptualization, S.F., S.C., F.C. and S.E.; Methodology, S.C., F.C., Y.H., F.P.D, D.N. and S.E.; Investigation, S.F., S.C, M.M. P, J.S., L.P., B.W., R.Z., D.N. and F.P.D., Formal Analysis, S.F., F.C., Y.H., S.C and S.E., Writing-Original Draft, S.F., F.C., Y.H and S.E., Writing-Review & Editing, S.F., W.H.W.T and S.E., Resources, L.P. and S.C., Funding Acquisition, S.E.

Conflict of interest

The author(s) declare that there is no conflict of interest.

Funding

The author(s) disclosed receipt of the following financial support for the research, authorship, and/or publication of this article: This work was supported by grants: HL60917, HL115008 and CTSA (UL1TR000439).

Ethical approval

The study was approved by the Cleveland Clinic Foundation Institutional Review Board, and written informed consent was obtained from all participants.

ORCID iD

Samar Farha https://orcid.org/0000-0003-4800-8928

Supplemental Material

Supplemental material for this article is available online.

References

1. Benza RL, Miller DP, Gomberg-Maitland M, et al. Predicting survival in pulmonary arterial hypertension: insights from the Registry to Evaluate Early and Long-Term Pulmonary Arterial Hypertension Disease Management (REVEAL). *Circulation* 2010; 122: 164–172.
2. Thenappan T, Shah SJ, Rich S, et al. Survival in pulmonary arterial hypertension: a reappraisal of the NIH risk stratification equation. *Eur Respir J* 2010; 35: 1079–1087.

3. Xu W, Janocha AJ and Erzurum SC. Metabolism in pulmonary hypertension. *Annu Rev Physiol* 2021; 83: 551–576.
4. Fessel JP, Hamid R, Wittmann BM, et al. Metabolomic analysis of bone morphogenetic protein receptor type 2 mutations in human pulmonary endothelium reveals widespread metabolic reprogramming. *Pulm Circ* 2012; 2: 201–213.
5. Rhodes CJ, Ghataorhe P, Wharton J, et al. Plasma metabolomics implicates modified transfer RNAs and altered bioenergetics in the outcomes of pulmonary arterial hypertension. *Circulation* 2017; 135: 460–475.
6. Zhao Y, Peng J, Lu C, et al. Metabolomic heterogeneity of pulmonary arterial hypertension. *PLoS One* 2014; 9: e88727.
7. Zhao YD, Chu L, Lin K, et al. A biochemical approach to understand the pathogenesis of advanced pulmonary arterial hypertension: metabolomic profiles of arginine, sphingosine-1-phosphate, and heme of human lung. *PLoS One* 2015; 10: e0134958.
8. Hernandez-Saavedra D, Sanders L, Freeman S, et al. Stable isotope metabolomics of pulmonary artery smooth muscle and endothelial cells in pulmonary hypertension and with TGF-beta treatment. *Sci Rep* 2020; 10: 413.
9. Xu W, Comhair SAA, Chen R, et al. Integrative proteomics and phosphoproteomics in pulmonary arterial hypertension. *Sci Rep* 2019; 9: 18623.
10. Brittain EL, Talati M, Fessel JP, et al. Fatty acid metabolic defects and right ventricular lipotoxicity in human pulmonary arterial hypertension. *Circulation* 2016; 133: 1936–1944.
11. Brittain EL, Niswender K, Agrawal V, et al. Mechanistic phase II clinical trial of metformin in pulmonary arterial hypertension. *J Am Heart Assoc* 2020; 9: e018349.
12. Farha S, Saygin D, Park MM, et al. Pulmonary arterial hypertension treatment with carvedilol for heart failure: a randomized controlled trial. *JCI Insight* 2017; 2 e95240.
13. Saygin D, Highland KB, Farha S, et al. Metabolic and functional evaluation of the heart and lungs in pulmonary hypertension by gated 2-[18F]-fluoro-2-deoxy-D-glucose positron emission tomography. *Pulm Circ* 2017; 7: 428–438.
14. Comhair SA, McDunn J, Bennett C, et al. Metabolomic endotype of asthma. *J Immunol* 2015; 195: 643–650.
15. Evans AM, DeHaven CD, Barrett T, et al. Integrated, nontargeted ultrahigh performance liquid chromatography/electrospray ionization tandem mass spectrometry platform for the identification and relative quantification of the small-molecule complement of biological systems. *Anal Chem* 2009; 81: 6656–6667.
16. Kalhan SC, Guo L, Edmison J, et al. Plasma metabolomic profile in nonalcoholic fatty liver disease. *Metabolism* 2011; 60: 404–413.
17. Kalhan SC, Gruca LL, Parimi PS, et al. Serine metabolism in human pregnancy. *Am J Physiol Endocrinol Metab* 2003; 284: E733–E740.
18. Garda HA, Arrese EL and Soulages JL. Structure of apolipophorin-III in discoidal lipoproteins. Interhelical distances in the lipid-bound state and conformational change upon binding to lipid. *J Biol Chem* 2002; 277: 19773–19782.
19. Tang WH, Tong W, Shrestha K, et al. Differential effects of arginine methylation on diastolic dysfunction and disease progression in patients with chronic systolic heart failure. *Eur Heart J* 2008; 29: 2506–2513.
20. Mor-Avi V, Lang RM, Badano LP, et al. Current and evolving echocardiographic techniques for the quantitative evaluation of cardiac mechanics: ASE/EAE consensus statement on methodology and indications endorsed by the Japanese Society of Echocardiography. *J Am Soc Echocardiogr* 2011; 24: 277–313.
21. Pirat B, McCulloch ML and Zoghbi WA. Evaluation of global and regional right ventricular systolic function in patients with pulmonary hypertension using a novel speckle tracking method. *Am J Cardiol* 2006; 98: 699–704.
22. Puwanant S, Park M, Popovic ZB, et al. Ventricular geometry, strain, and rotational mechanics in pulmonary hypertension. *Circulation* 2010; 121: 259–266.
23. Rudski LG, Lai WW, Afilalo J, et al. Guidelines for the echocardiographic assessment of the right heart in adults: a report from the American Society of Echocardiography endorsed by the European Association of Echocardiography, a registered branch of the European Society of Cardiology, and the Canadian Society of Echocardiography. *J Am Soc Echocardiogr* 2010; 23: 685–713; quiz 786–688.
24. Sachdev A, Villarraga HR, Frantz RP, et al. Right ventricular strain for prediction of survival in patients with pulmonary arterial hypertension. *Chest* 2011; 139: 1299–1309.
25. Farha S, Lundgrin EL and Erzurum SC. Novel therapeutic approaches to preserve the right ventricle. *Curr Heart Fail Rep* 2013; 10: 12–17.
26. Benjamini Y HY. Controlling the false discovery rate: a practical and powerful approach to multiple testing. *J R Stat Soc Series B* 1995; 57(1): 289–300.
27. Rolland T, Tasan M, Charloteaux B, et al. A proteome-scale map of the human interactome network. *Cell* 2014; 159: 1212–1226.
28. Rual JF, Venkatesan K, Hao T, et al. Towards a proteome-scale map of the human protein-protein interaction network. *Nature* 2005; 437: 1173–1178.
29. Cheng F, Desai RJ, Handy DE, et al. Network-based approach to prediction and population-based validation of in silico drug repurposing. *Nat Commun* 2018; 9: 2691.
30. Hu J, Rho HS, Newman RH, et al. PhosphoNetworks: a database for human phosphorylation networks. *Bioinformatics* 2014; 30: 141–142.
31. Cheng F, Jia P, Wang Q, et al. Quantitative network mapping of the human kinome interactome reveals new clues for rational kinase inhibitor discovery and individualized cancer therapy. *Oncotarget* 2014; 5: 3697–3710.
32. Keshava Prasad TS, Goel R, Kandasamy K, et al. Human protein reference database – 2009 update. *Nucleic Acids Res* 2009; 37: D767–D772.
33. Hornbeck PV, Zhang B, Murray B, et al. PhosphoSitePlus, 2014: mutations, PTMs and recalibrations. *Nucleic Acids Res* 2015; 43: D512–D520.
34. Lu CT, Huang KY, Su MG, et al. DbPTM 3.0: an informative resource for investigating substrate site specificity and functional association of protein post-translational modifications. *Nucleic Acids Res* 2013; 41: D295–D305.
35. Dinkel H, Chica C, Via A, et al. Phospho.ELM: a database of phosphorylation sites–update 2011. *Nucleic Acids Res* 2011; 39: D261–D267.
36. Oughtred R, Stark C, Breitkreutz BJ, et al. The BioGRID interaction database: 2019 update. *Nucleic Acids Res* 2019; 47: D529–D541.

37. Cowley MJ, Pinese M, Kassahn KS, et al. PINA v2.0: mining interactome modules. *Nucleic Acids Res* 2012; 40: D862–D865.
38. Meyer MJ, Das J, Wang X, et al. INstruct: a database of high-quality 3D structurally resolved protein interactome networks. *Bioinformatics* 2013; 29: 1577–1579.
39. Licata L, Briganti L, Peluso D, et al. MINT, the molecular interaction database: 2012 update. *Nucleic Acids Res* 2012; 40: D857–D861.
40. Orchard S, Ammari M, Aranda B, et al. The MIntAct project–IntAct as a common curation platform for 11 molecular interaction databases. *Nucleic Acids Res* 2014; 42: D358–D363.
41. Breuer K, Foroushani AK, Laird MR, et al. InnateDB: systems biology of innate immunity and beyond–recent updates and continuing curation. *Nucleic Acids Res* 2013; 41: D1228–D1233.
42. Csabai L, Olbei M, Budd A, et al. SignaLink: multilayered regulatory networks. *Methods Mol Biol* 2018; 1819: 53–73.
43. Huttlin EL, Ting L, Bruckner RJ, et al. The BioPlex network: a systematic exploration of the human interactome. *Cell* 2015; 162: 425–440.
44. Cheng F, Kovacs IA and Barabasi AL. Network-based prediction of drug combinations. *Nat Commun* 2019; 10: 1197.
45. Kanehisa M, Sato Y, Furumichi M, et al. New approach for understanding genome variations in KEGG. *Nucleic Acids Res* 2019; 47: D590–D595.
46. Brunk E, Sahoo S, Zielinski DC, et al. Recon3D enables a three-dimensional view of gene variation in human metabolism. *Nat Biotechnol* 2018; 36: 272–281.
47. Pornputtapong N, Nookaew I and Nielsen J. Human metabolic atlas: an online resource for human metabolism. *Database (Oxford)* 2015; 2015: bav068.
48. Mura M, Cecchini MJ, Joseph M, et al. Osteopontin lung gene expression is a marker of disease severity in pulmonary arterial hypertension. *Respirology* 2019; 24: 1104–1110.
49. Lopatin Y. Metabolic therapy in heart failure. *Card Fail Rev* 2015; 1: 112–117.
50. Tsai SY, Wu YW, Wang SY, et al. Clinical significance of quantitative assessment of right ventricular glucose metabolism in patients with heart failure with reduced ejection fraction. *Eur J Nucl Med Mol Imaging* 2019; 46: 2601–2609.
51. Oikawa M, Kagaya Y, Otani H, et al. Increased [18F]fluorodeoxyglucose accumulation in right ventricular free wall in patients with pulmonary hypertension and the effect of epoprostenol. *J Am Coll Cardiol* 2005; 45: 1849–1855.
52. Bokhari S, Raina A, Rosenweig EB, et al. PET imaging may provide a novel biomarker and understanding of right ventricular dysfunction in patients with idiopathic pulmonary arterial hypertension. *Circ Cardiovasc Imaging* 2011; 4: 641–647.
53. Ohira H, deKemp R, Pena E, et al. Shifts in myocardial fatty acid and glucose metabolism in pulmonary arterial hypertension: a potential mechanism for a maladaptive right ventricular response. *Eur Heart J Cardiovasc Imaging* 2016; 17: 1424–1431.
54. Wang TJ and Gupta DK. Metabolite profiles in heart failure: looking for unique signatures in a heterogeneous syndrome. *J Am Coll Cardiol* 2015; 65: 1521–1524.
55. Cheng ML, Wang CH, Shiao MS, et al. Metabolic disturbances identified in plasma are associated with outcomes in patients with heart failure: diagnostic and prognostic value of metabolomics. *J Am Coll Cardiol* 2015; 65: 1509–1520.
56. Xu W, Koeck T, Lara AR, et al. Alterations of cellular bioenergetics in pulmonary artery endothelial cells. *Proc Natl Acad Sci U S A* 2007; 104: 1342–1347.
57. Fijalkowska I, Xu W, Comhair SAA, et al. Hypoxia inducible-factor1alpha regulates the metabolic shift of pulmonary hypertensive endothelial cells. *Am J Pathol* 2010; 176: 1130–1138.
58. Farha S, Asosingh K, Xu W, et al. Hypoxia-inducible factors in human pulmonary arterial hypertension: a link to the intrinsic myeloid abnormalities. *Blood* 2011; 117: 3485–3493.
59. Bonnet S, Michelakis ED, Porter CJ, et al. An abnormal mitochondrial-hypoxia inducible factor-1α-Kv channel pathway disrupts oxygen sensing and triggers pulmonary arterial hypertension in fawn hooded rats: similarities to human pulmonary arterial hypertension. *Circulation* 2006; 113: 2630–2641.
60. Bujak R, Mateo J, Blanco I, et al. New biochemical insights into the mechanisms of pulmonary arterial hypertension in humans. *PLoS One* 2016; 11: e0160505.